

Microscopic Origin of Frictional Rheology in Dense Suspensions

Kabir Ramola

Martin Fisher School of Physics,
Brandeis University

In collaboration with

Jetin Thomas, Abhinendra Singh, Romain Mari,
Jeffrey Morris and Bulbul Chakraborty

December 4, 2018

- 1 Discontinuous Shear Thickening
- 2 Constitutive Laws
- 3 Mean Field Theory
- 4 Simulations of Dense Suspensions
- 5 Microscopic Theory

Some Definitions

- **Shear Rate:** $\dot{\gamma}$
- **Stress Tensor:**

$$\hat{\sigma} = \begin{pmatrix} \sigma_{xx} & \sigma_{xy} \\ \sigma_{yx} & \sigma_{yy} \end{pmatrix} \quad (1)$$

- **Shear Stress:** $\sigma \equiv \sigma_{xy}$
- **Pressure:** $2P = \text{Tr}(\hat{\sigma}) = \sigma_{xx} + \sigma_{yy}$
- **Stress Anisotropy:** $\mu = \frac{\lambda_+ - \lambda_-}{\lambda_+ + \lambda_-} \equiv \frac{\tau}{2P} \approx \frac{\sigma_{xy}}{P}$
- **Viscosity:** $\eta = \frac{d\sigma_{xy}}{d\dot{\gamma}}$

- 1 Discontinuous Shear Thickening
- 2 Constitutive Laws
- 3 Mean Field Theory
- 4 Simulations of Dense Suspensions
- 5 Microscopic Theory

Discontinuous Shear Thickening

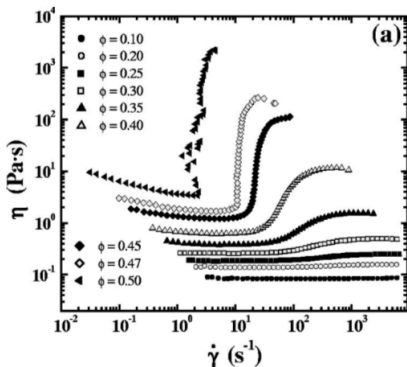
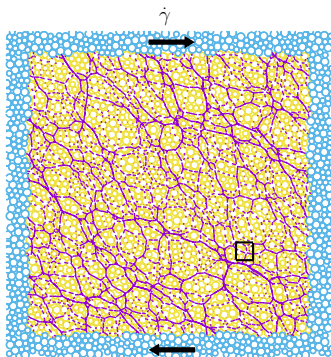


Figure: (Left) A snapshot of a suspension of 2000 soft frictional disks sheared at a variable rate $\dot{\gamma}$, with the shear stress $\sigma \equiv \sigma_{xy}$ held fixed. (Right) Viscosity vs Shear rate for 500nm calcium carbonate + polymer brush in PEG 200 R. G. Egres and Norman J. Wagner *Journal of Rheology* 49, 719 (2005).

Outline

- 1 Discontinuous Shear Thickening
- 2 Constitutive Laws**
- 3 Mean Field Theory
- 4 Simulations of Dense Suspensions
- 5 Microscopic Theory

Constitutive Laws: $\mu(I)$ Rheology

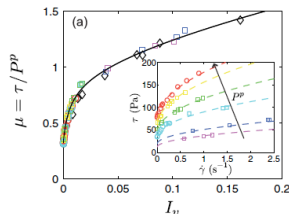


Figure: Observed **Stress Anisotropy** $\mu = \tau/2P$ from several experiments of dense suspensions. F. Boyer, E. Guazzelli, and O. Pouliquen, *Physical Review Letters* 107, 188301 (2011).

- μ depends on the viscous number $I_v \equiv \frac{\eta \dot{\gamma}}{P}$
- I_v depends on the packing fraction ϕ : $I_v(\phi) \propto (\phi_J - \phi)^2$.
- In the limit of small I_v is: $\mu - \mu_c \simeq I_v^{1/2}$, (μ_c depends weakly on the properties of the grains J. Dong and M. Trulsson, *Physical Review Fluids* 2, 081301 (2017)).

- We can therefore infer/postulate

$$\eta(\phi, \sigma_{xy}) \propto \frac{\mu(\phi, \sigma_{xy})}{(\mu(\phi, \sigma_{xy}) - \mu_c)^2}. \quad (2)$$

- The **DST boundary** is given by the equation

$$\frac{d\dot{\gamma}}{d\sigma_{xy}} = 0. \quad (3)$$

- Which translates to the following equation **in terms of the stress anisotropy**:

$$\frac{\sigma_{xy}}{\mu} \left| \frac{d\mu}{d\sigma_{xy}} \right| = \frac{\mu - \mu_c}{\mu + \mu_c}. \quad (4)$$

Outline

- 1 Discontinuous Shear Thickening
- 2 Constitutive Laws
- 3 Mean Field Theory**
- 4 Simulations of Dense Suspensions
- 5 Microscopic Theory

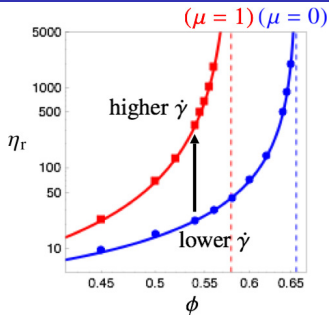


Figure: Two branches of viscosity: lower (lubricated, friction coefficient $\mu = 0$) and upper (frictional, $\mu = 1$).

- Use constitutive laws for the two branches (Smooth/Rough):

$$\phi = \Phi_s(l_v) \quad ; \quad \sigma/P = \mu_s(l_v), \quad (5)$$

$$\phi = \Phi_r(l_v) \quad ; \quad \sigma/P = \mu_r(l_v). \quad (6)$$

Mean Field Theory (Cont.)

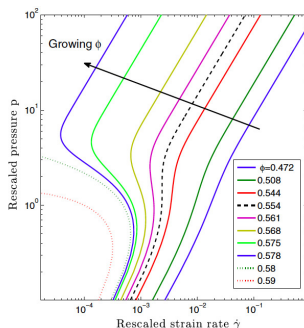


Figure: Predictions of the Wyart and Cates model for increasing solid fraction.

- Interpolate with a p -dependent jamming density $\phi_J(p)$:

$$P = \lambda \dot{\gamma} (\phi_J(p) - \phi)^{-2} \quad (7)$$

$$\phi_J(p) = \phi_m f + \phi_0 (1 - f) \quad (8)$$

Phase Diagram

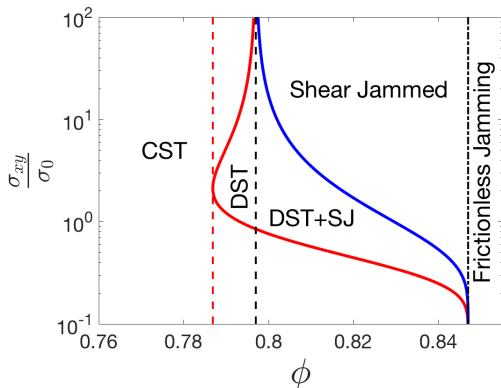


Figure: Phase diagram in the shear stress–packing fraction (σ_{xy}, ϕ) plane. The left (red) curve locates the points where $\frac{d\dot{\gamma}}{d\sigma_{xy}} = 0$. The right (blue) curve shows packing fraction dependent maximal stress above which the suspension is shear-jammed, i.e., above which no flowing states exist.

- 1 Discontinuous Shear Thickening
- 2 Constitutive Laws
- 3 Mean Field Theory
- 4 Simulations of Dense Suspensions**
- 5 Microscopic Theory

Simulating Dense Suspensions

- We perform simulations of simple shear under **constant stress** of a monolayer of $N = 2000$ bidisperse (radii a and $1.4a$) spherical particles following [R. Mari, R. Seto, J. F. Morris, and M. M. Denn, Journal of Rheology 58, 1693 \(2014\)](#).
- These follow an **overdamped dynamics** and are subject to **Stokes drag**, pairwise lubrication, frictional contact, and short-range repulsive forces.
- Because of the repulsive force of maximum F_0 at contact, **frictional contacts only form for stresses about or larger than** $\sigma_0 \equiv F_0/a^2$, which induces DST at volume fractions $\phi \gtrsim 0.78$.

Observed Stress Anisotropy

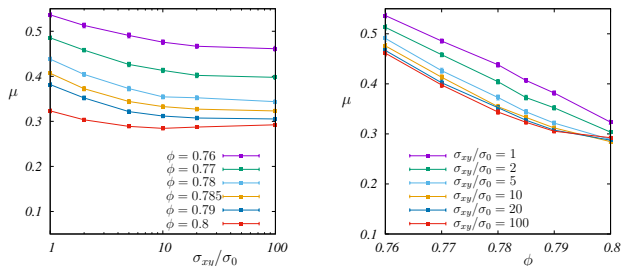


Figure: Observed $\mu = \tau/2P$ from simulations of suspensions J. E. Thomas, K. Ramola, A. Singh, R. Mari, J. Morris, B. Chakraborty, Phys. Rev. Lett. **121**, 128002 (2018).

Testing the Constitutive Relation

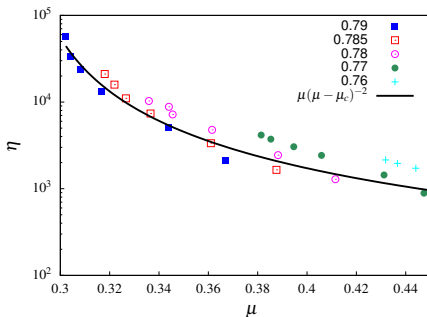


Figure: Plot of the viscosity, $\eta(\phi, \sigma_{xy})$ vs $\mu(\phi, \sigma_{xy})$ for different packing fractions, obtained from the simulations (symbols) compared to the constitutive relation $\eta = \mu / (\mu - \mu_c)^2$. Here $\mu_c = 0.285$, is chosen to be the lowest value of the stress anisotropy observed in the simulations. The viscosity η is measured in units of η_0 , the viscosity of the underlying Newtonian fluid, and in our simulations we set $\eta_0 = 1$.

Outline

- 1 Discontinuous Shear Thickening
- 2 Constitutive Laws
- 3 Mean Field Theory
- 4 Simulations of Dense Suspensions
- 5 Microscopic Theory**

Ingredients for a Microscopic Theory

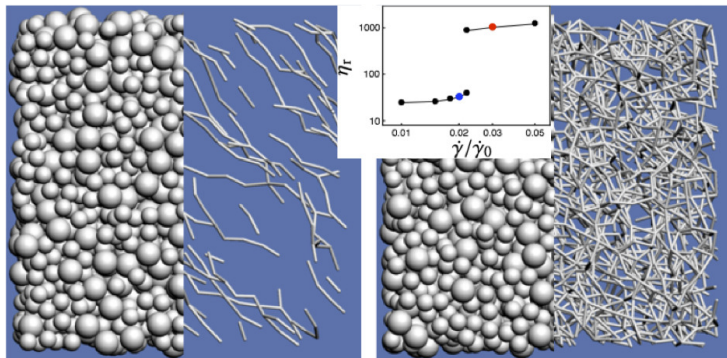
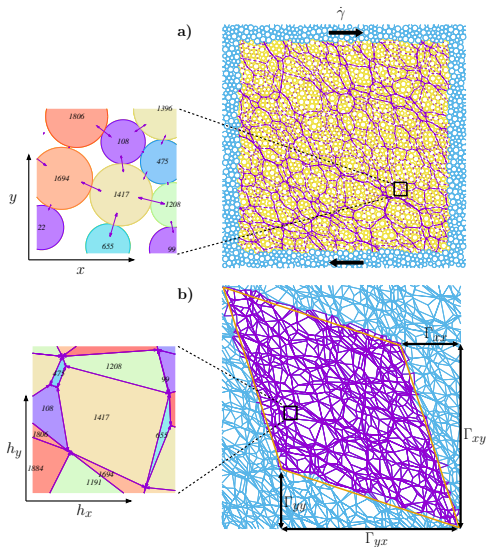


Figure: Instantaneous particle configurations and frictional contact force networks from simulation (Seto et al. 2013) for the low viscosity (**left**) and high viscosity states (**right**) highlighted in color in the inset. R. Seto, R. Mari, J. F. Morris, M. M. Denn, *Phys. Rev. Lett.* **111**, 218301 (2013)

Phys. Rev. Lett. **111**, 218301 (2013)

Height Space Representation



Macroscopic Stress Tensor

- In the continuum, the local stress tensor is $\hat{\sigma} = \nabla \times \vec{h}$:

$$\hat{\sigma} = \begin{pmatrix} \partial_y h_x & \partial_y h_y \\ -\partial_x h_x & -\partial_x h_y \end{pmatrix}; \quad \hat{\Sigma} = \begin{pmatrix} L_y \Gamma_{yx} & L_y \Gamma_{yy} \\ -L_x \Gamma_{xx} & -L_x \Gamma_{xy} \end{pmatrix}, \quad (9)$$

where $\hat{\Sigma}$ is the virial or the **global force moment tensor**.

- The **shear stress is held fixed** with

$$\Gamma_{yy} = -\Gamma_{xx} = \sigma \quad (10)$$

- The **pressure** and the **normal stress** are

$$2P = \lambda_+ + \lambda_- = \Gamma_{yx} - \Gamma_{xy}; \quad N_1 = \Sigma_{xx} - \Sigma_{yy} = \Gamma_{yx} + \Gamma_{xy}. \quad (11)$$

- The **stress anisotropy** μ is

$$\mu = \frac{\tau}{2P} = \frac{\sqrt{(N_1)^2 + 4\sigma^2}}{2P} \approx \frac{\sigma}{P}. \quad (12)$$

- Using the force tiling representation, we compute the **Pair Correlation Function of Vertices**, defined to be

$$g_2(\vec{h}) = \left\langle \frac{A}{N_v(N_v - 1)} \sum_{i=1}^{N_v} \sum_{j \neq i}^{N_v} \delta(\vec{h} - (\vec{h}_i - \vec{h}_j)) \right\rangle, \quad (13)$$

where N_v is the total number of voids in the system, $A = |\vec{\Gamma}_x \times \vec{\Gamma}_y|$, and $\rho_v = N_v/A$ is the density of height vertices in the force tiling.

- These are averaged over 200 configurations obtained from the simulated steady state of dense suspensions at each ϕ and σ_{xy} .

Observed Pair Correlations

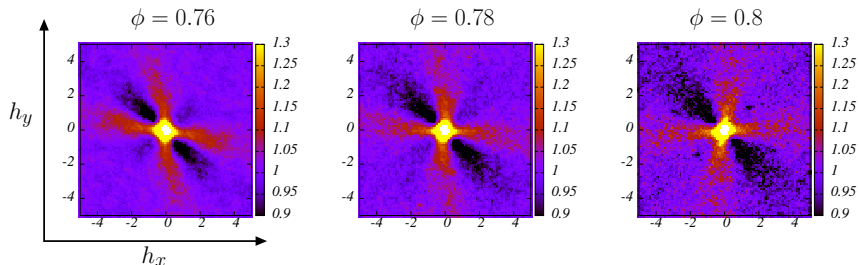


Figure: Observed pair correlation functions at $\sigma_{xy} = 2$, at packing fractions $\phi = 0.76, 0.78$ and 0.8 . The forces (and consequently the heights) have been scaled by the imposed shear stress σ . The change in symmetry of $g_2(\vec{h})$ is clearly visible as the packing fraction is increased.

Constructing a Thermal Ensemble

- Using the pair correlations we can construct a **potential**

$$V_2(\vec{h}) = -\log \left(\frac{g_2(\vec{h})}{g_2(|\vec{h}|)} \right), \quad (14)$$

that induces an **anisotropy in the interactions** based on the observed correlation functions.

- The ensemble of configurations that are sampled in the non-equilibrium dynamics are assumed to obey a **statistical mechanical description**, with each configuration \mathcal{C} occurring with a **probability** $p(\mathcal{C}) \propto \exp(-V(\mathcal{C}))$. J. E. Thomas, K. Ramola, A. Singh, R. Mari, J. Morris, B. Chakraborty, Phys. Rev. Lett. **121**, 128002 (2018).

- Shear stress sets the **pressure scale** (and Area): we control this by a **Lagrange multiplier** $f_p^*(\sigma)$.
- The **partition function** of the system is given by

$$\begin{aligned} Z_{\phi,\sigma} &= \frac{1}{N_v!} \int_0^\infty dA \exp(-N_v f_p^* A) \times \\ &\quad \underbrace{\int_A \prod_{i=1}^{N_v} d\vec{h}_i \exp\left(-\sum_{i,j} V_{\phi,\sigma}(\vec{h}_i - \vec{h}_j)\right)}_{A^{N_v} \exp(-\epsilon_{\phi,\sigma}(A, N_v))}, \\ &= \int_0^\infty dA \exp(-\mathcal{F}_{A;\phi,\sigma}). \end{aligned} \tag{15}$$

where the positions \vec{h}_i are confined to be within the box defined by $A \equiv (\vec{\Gamma}_x, \vec{\Gamma}_y)$.

Testing the Potentials

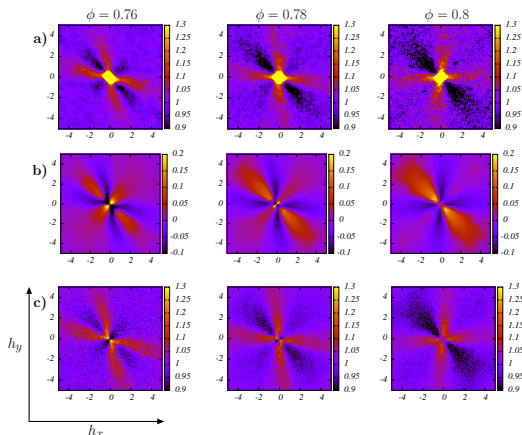


Figure: **a)** Observed pair correlation functions at $\sigma_{xy} = 2$, at packing fractions $\phi = 0.76, 0.78$ and 0.8 . **b)** Potentials constructed using these pair correlation functions. **c)** A comparison with pair correlations obtained from direct Monte Carlo simulations of particles interacting via these potentials.

Sampling the Energy Function

- We perform a **Monte Carlo sampling** of the energy function

$$f(\mu; \phi, \sigma) \equiv \mathcal{F}/N_v = f_p^* \sigma^2 \left(\frac{1}{\mu^2} - 1 \right) - \log \left[\sigma^2 \left(\frac{1}{\mu^2} - 1 \right) \right] + \frac{\epsilon_{\phi, \sigma}(\mu, N_v)}{N_v}.$$

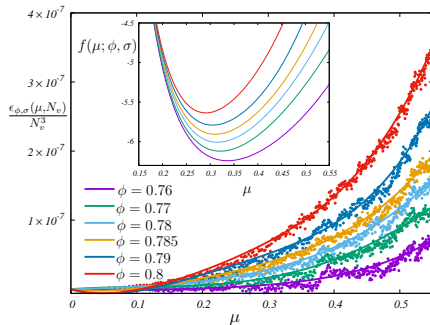


Figure: Sampled values of $\epsilon_{\phi, \sigma}(\mu, N_v)$ for $N_v = 1024$ and $\sigma_{xy}/\sigma_0 = 100$, with V_2 derived from simulations at different packing fractions ϕ . **(Inset)** $f(\mu; \phi, \sigma)$ for $N_v = 3000$, and $f_p^* = 6.5 \times 10^{-4}$.

Predictions

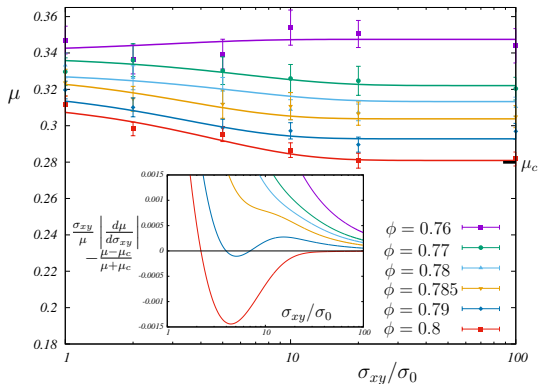


Figure: Variation of the macroscopic friction coefficient μ , corresponding to the minimum of the free energy function. We find that μ decreases as packing fraction ϕ and the confining shear stress σ_{xy} are increased. **(Inset)** Plot showing the appearance of two solutions at $\phi = 0.79$, and the second solution moving out to $\sigma_{xy} \rightarrow \infty$ at $\phi = 0.8$.

Summary and Conclusions

- We have identified a **correlation function that exhibits significant changes** in anisotropy across the DST transition.
- The correlations are in force space, and reflect the **collective behavior** triggered by changes in the nature of the *contact forces*.
- Remarkably, a theory based on pair potentials in **force space describes the macroscopic rheology**.
- The decrease in μ indicates that the pressure increase for an imposed increase of shear stress is **larger in the frictional branch** of DST than it is in the frictionless branch of DST.

Thank You.